Effects of wind and traffic excitation on the mode identifiability of a cable-stayed bridge

*Wen-Hwa Wu[1)], Sheng-Wei Wang[2)], Chien-Chou Chen[3)] and Gwolong Lai[3)]

[1), 2), 3)]*Department of Construction Engineering, NYUST, Yunlin 640,Taiwan*
[1)] *wuwh@yuntech.edu.tw*

ABSTRACT

Deficient modes that cannot be always identified from different sets of measurement data may exist in the application of operational modal analysis such as the stochastic subspace identification (SSI) techniques in large-scale civil structures. For systematically assessing this problem associated with Ting Kau Bridge, a recently developed SSI algorithm based on an alternative stabilization diagram and a hierarchical sifting process is extended and applied in this research to investigate several sets of monitoring data. The evaluation of delicately selected cases clearly distinguishes the effect of traffic excitation on the identifiability of the targeted deficient mode from the effect of wind excitation. Careful inspection on the shape vector of the deficient mode under different excitation conditions leads to the postulation that this mode is actually induced by the motion of the central tower. The analysis incorporating the tower measurements solidly verifies this postulation by yielding the prevailing components at the tower locations in the extended mode shape vector. Moreover, it is also confirmed that this mode can be stably identified under all the circumstances with the addition of tower measurements.

1. INTRODUCTION

Among all the output-only identification methods, stochastic subspace identification (SSI) has been gaining more popularity in recent years due to its strict mathematical basis and excellent applicability in various systems. The widely employed formulation of SSI was first suggested by Van Overschee and De Moor (1991) and the corresponding algorithm for modal parameter identification was also established by them in the subsequent few years. A number of core techniques in linear algebra such as RQ (or LQ) decomposition, singular value decomposition (SVD), and oblique

---

[1)] Professor
[2)] Postdoctoral Research Associate
[3)] Associate Professor

projection were utilized in their theoretical derivation and solution algorithm. Because of directly processing the output matrix from measurements, this series of methods are typically referred as the data-driven SSI. In addition to the data-driven SSI, the other type of covariance-driven SSI was initially proposed by Peeters (2000) to conduct SSI with the covariance matrix of output measurements. The covariance-driven SSI is relatively simple in mathematical derivation and generally efficient in computation since it only involves with SVD. Even with the help of stabilization diagram, appropriate discrimination criteria according to theories like clustering analysis need to be further established such that systematic extraction of effective physical modes can be attained to reach the ultimate goal of an automated SSI analysis (Reynders *et al*. 2012, Ubertini *et al*. 2013).

The application of operational modal analysis such as the SSI techniques in large-scale civil structures, however, still encounters difficulties under certain circumstances. For instance, deficient modes that cannot be identified all the time from different sets of measurement data may exist. Even for the cases where the identification of these deficient modes is feasible, the obtained modal parameters can be relatively diversified in comparison to the other robust modes. Such inconsistent results may seriously deteriorate the reliability of the subsequent damage detection using an on-line structural health monitoring (SHM) system to conduct automatic modal identification. Therefore, it is extremely important to validate the fidelity of the identified modal parameters for these deficient modes before they are exploited in vibration-based damage detection. Nevertheless, there is no theoretical or even empirical criterion available for the identifiability of modes in performing the operational modal analysis with ambient vibration measurements. Making use of the long-term monitoring data of ambient vibration responses acquired from the instrumented Ting Kau Bridge (TKB) in Hong Kong under different wind excitation conditions, Ni *et al*. (2015) started a pioneering work in probing the mode identifiability with the data-driven SSI algorithm. It was discovered that a deficient mode is identifiable with consistent mode shape vectors under typhoon conditions, but not identifiable under weak wind conditions. Furthermore, a threshold value of mean hourly wind speed (7.5 m/sec) was obtained to ensure a reliable identification of this deficient mode.

Attempting to attack the problem that the application of conventional SSI techniques to identify the modal parameters of a stay cable usually leads to a failure, a recent work by the authors (Wu *et al*. 2014, 2016) established an improved algorithm based on the covariance-driven SSI. An alternative stabilization diagram was first proposed to more conveniently stand out stable modal parameters and a hierarchical sifting process was then developed to systematically extract reliable modal parameters from the alternative stabilization diagram. Demonstrated by analyzing the ambient vibration measurements of real stay cables, the feasibility of this new approach was verified with successfully obtaining the modal frequencies, damping ratios, and mode shape ratios for almost all the cable modes in the examined frequency range. Equipped with this improved SSI algorithm, the current study aims to extensively assess the mode identifiability problem by delving into its mechanism behind. A preliminary analysis of known data sets is first conducted to recognize the importance of considering the traffic excitations along with the wind excitations, followed by analyzing several data sets under different excitation conditions with the improved SSI algorithm

to postulate a vibration mechanism for the targeted deficient mode. Finally, the measurements at the central tower are further incorporated in the SSI analysis for directly verifying this mechanism deduced from the deck measurements.

2. SENSOR SETUP AND INVESTIGATED DATA SETS OF TING KAU BRIDGE

Ting Kau Bridge, as shown in Fig. 1, is a thee-tower cable-stayed bridge connecting Tsing Yi and Ting Kau located in Hong Kong. It consists of two main spans (448 m+475 m) and two side spans (127 m+127 m) to have a total length of 1177 m. In the transverse direction, the deck is supported at the three towers, the pier at the Ting Kau end, and the abutment at the Tsing Yi end. Moreover, the deck is merely restrained at the central tower in the longitudinal direction. The three slender single-column towers of TKB are with heights of 170 m (Ting Kau Tower), 194 m (Central Tower), and 158 m (Tsing Yi Tower), respectively. The cable system is arranged in four planes and all the 384 stay cables are anchored to the deck edge girders at 13.5 m intervals. Eight longitudinal stabilizing cables, up to 464.6 m long and diagonally connecting the top of the central tower to the deck adjacent to side towers, are designed to restrain the central tower from traffic and vertical wind loading.

The sensors permanently installed on TKB include 45 accelerometers, 7 anemometers, 2 displacement transducers, 83 temperature sensors, 88 strain gauges and 6 weigh-in-motion sensors. In this section, description will only cover the deployment of the accelerometers and anemometers related to the measurements adopted in the current study. As illustrated in Fig. 1, there are three propeller-type anemometers installed at the top of each tower. Besides, four ultrasonic-type anemometers were installed on both sides of the deck at Sections E and L. The sampling frequency of all the anemometers was set at 2.56Hz. Fig. 1 also displays that a total of 24 uni-axial accelerometers were employed to measure the vibration signals at eight deck sections of TKB. Furthermore, four bi-axial accelerometers were used to record the acceleration histories at the top of each tower and at the base of central tower. The detailed arrangement of the accelerometers installed on the bridge deck is plotted in Fig. 2. It should be noted that the accelerometers (2, 5, 8, 11, 14, 17, 20, and 23) installed along the central line of deck measure the transverse (*y*-direction) acceleration and those (1, 3, 4, 6, 7, 9, 10, 12, 13, 15, 16, 18, 19, 21, 22, and 24) installed at both sides of deck collect the vertical (*z*-direction) response. The sampling frequency of all the accelerometers was set at 25.6Hz.

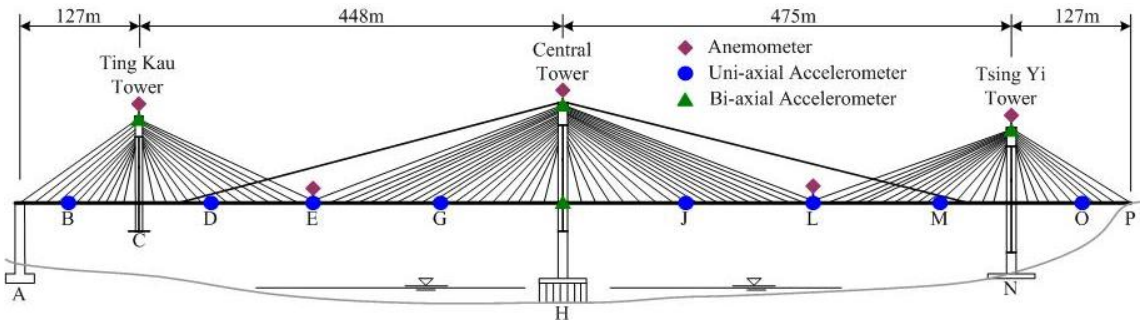

Fig. 1 Ting Kau Bridge and its sensor locations

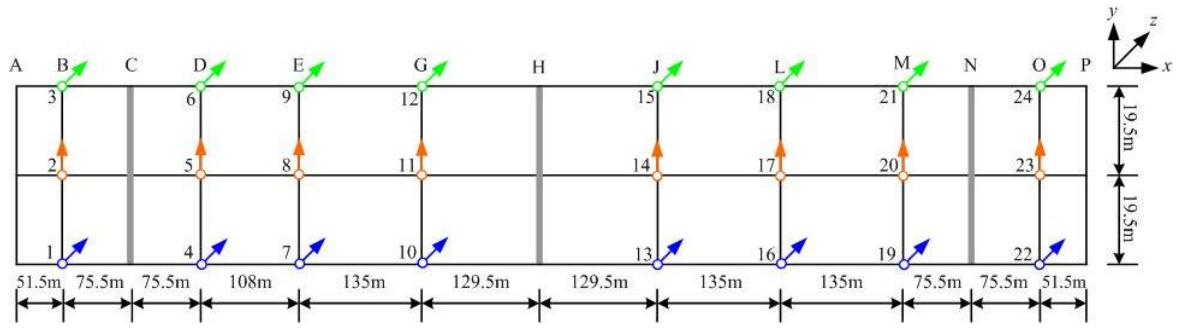

Fig. 2 Detailed arrangement of accelerometers on bridge deck

Table 1 Description of 10 data sets selected under different wind excitation conditions

Condition	Case	Time Duration	Mean Hourly Wind Speed (m/sec)
Normal	N1	15:00-16:00, 28 Dec 1999	2.00
	N2	15:00-16:00, 18 Feb 1999	3.40
	N3	15:00-16:00, 01 Mar 1999	3.34
	N4	15:00-16:00, 21 Jun 1999	3.41
	N5	15:00-16:00, 24 Jul 1999	6.17
	N6	15:00-16:00, 12 Aug 1999	4.20
Typhoon	Maggie	03:00-04:00, 07 Jun 1999	12.11
	Sam	02:00-03:00, 23 Aug 1999	15.62
	York 1	06:00-07:00, 16 Sep 1999	21.72
	York 2	15:00-16:00, 16 Sep 1999	17.91

In this study, 10 sets of 1-hour acceleration records collected from the 24 accelerometers deployed on the bridge deck in 1999 are investigated. Based on the associated mean hourly wind speed calculated with the data from the anemometers located on the windward side of the deck (Ni *et al*. 2015), these data sets can be classified into two different wind excitation conditions. As listed in Table 1, 6 sets are under the normal (weak) wind condition with their mean hourly speeds all less than 7.5 m/sec and will be referred as Cases N1 to N6. On the other hand, 4 sets are under the typhoon (strong) wind condition with their mean hourly speeds far beyond 7.5 m/sec and will be labeled with the names of their corresponding typhoons.

3. PRELIMINARY ANALYSIS

Before assessing the mode identifiability problem with the improved SSI algorithm,

a preliminary analysis is first performed on the 10 data sets to assemble more vibration characteristics of TKB under different excitation conditions. The acceleration records of Sensors 10 and 11 located at Section G are examined herein to represent the vertical and transverse responses of bridge deck, respectively. Case N1 under weak wind condition and Case Sam under strong wind condition are taken for illustrating three distinctive wind excitations. Figs. 3 and 4 depict the corresponding time histories and Fourier amplitude spectra (FAS), respectively. From Fig. 3, it is clear that the vertical response is generally larger than the transverse response at the deck of TKB. More importantly, both the vertical and transverse responses of Case N1 are much greater than the corresponding quantities of Case Sam. This phenomenon apparently indicates that the deck response is mainly induced by the passing traffic. Under the typhoon condition, the traffic is certainly decreased or even restricted such that the deck vibration is significantly reduced. The FAS in Fig. 4 over the low frequency range from 0 to 0.5 Hz further discloses the identifiability for the first few major modes of bridge deck under different excitation conditions. First of all, the mode with a frequency of 0.165 Hz is dominant in the vertical FAS under all the excitation cases. This mode has been identified as the first vertically bending mode (Ni *et al*. 2015) and will be referred as BV1 in this work. The other mode with a frequency of 0.227 Hz is the target of this study to investigate the mode identifiability and can only be easily distinguished in the vertical FAS for Case Sam. With the demonstration in the subsequent sections that this mode is principally induced by the motion of the central tower, it is consequently signified as CT. As for the examination of the corresponding transverse FAS, it provides a clear identification for the mode with a frequency of 0.258 Hz under all the excitation cases. This mode has also been identified as the first horizontally bending mode (Ni *et al*. 2015) and will be denoted as BH1. It will be focused on the three major modes (BV1, CT, and BH1) mentioned above to investigate the mode identifiability problem in the current work.

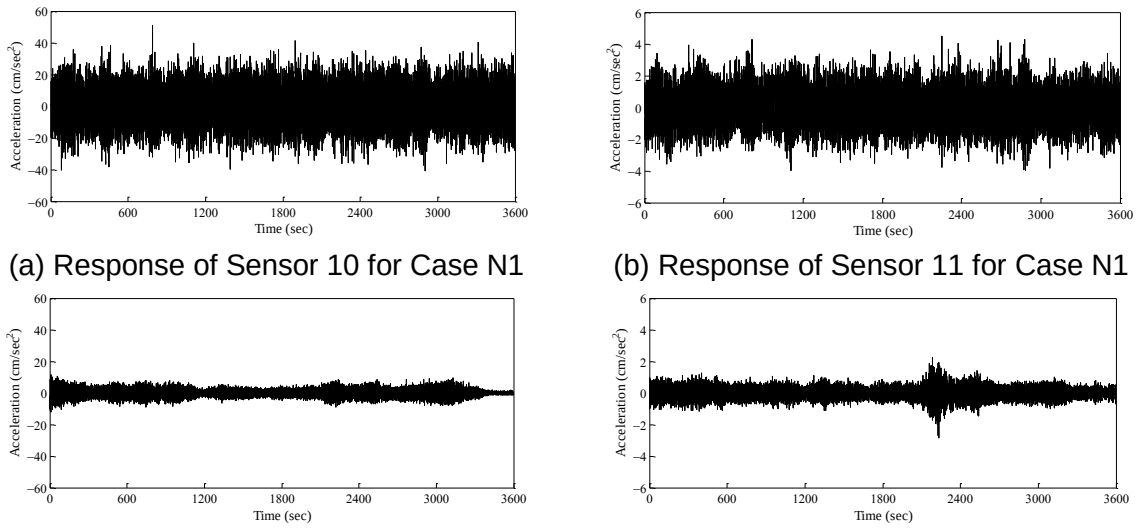

(a) Response of Sensor 10 for Case N1

(b) Response of Sensor 11 for Case N1

(c) Response of Sensor 10 for Case Sam

(d) Response of Sensor 11 for Case Sam

Fig. 3 Time histories of Sensors 10 and 11 under various wind conditions

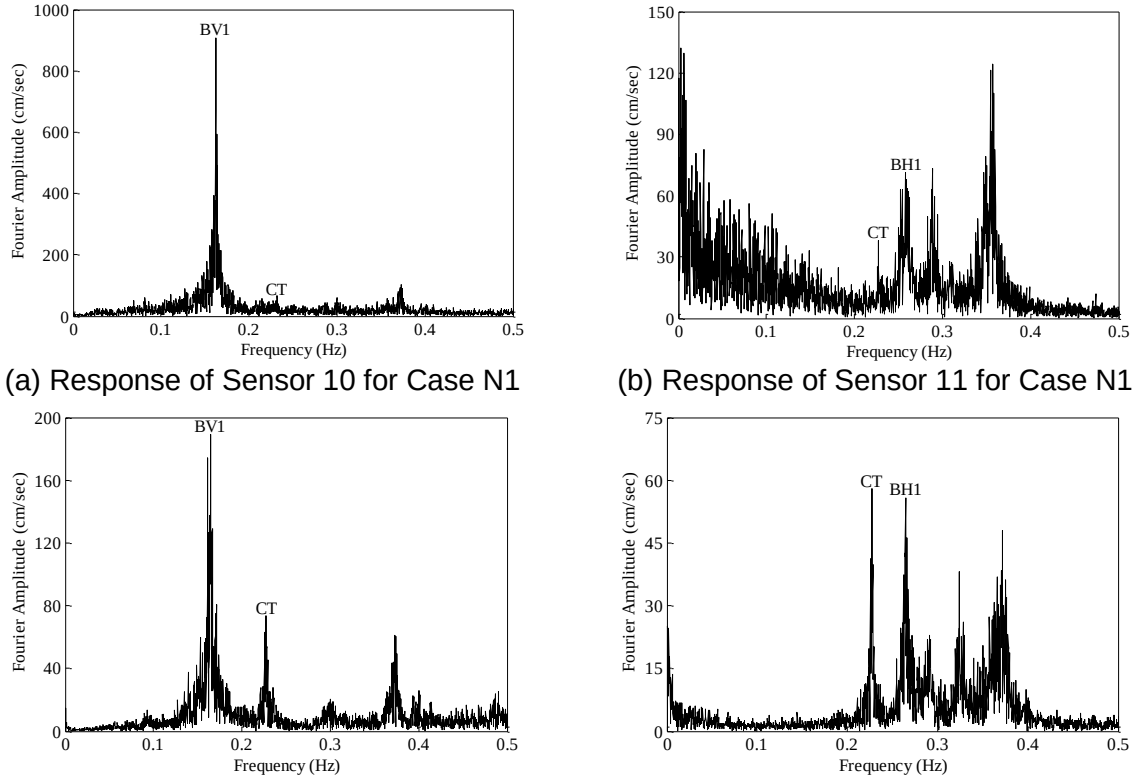

(a) Response of Sensor 10 for Case N1

(b) Response of Sensor 11 for Case N1

(c) Response of Sensor 10 for Case Sam

(d) Response of Sensor 11 for Case Sam

Fig. 4 Fourier amplitude spectra of Sensors 10 and 11 under various wind conditions

4. IMPROVED SSI ALGORITHM FOR MODAL PARAMETER IDENTIFICATION

The usually encountered problem for the applications of SSI techniques in large-scale civil structures is that the process noise and measurement noise of a real structure generally do not satisfy all the zero-mean, white-noise, and stationary assumptions on which the derivation of SSI is based. This discrepancy between theoretical simplification and actual complexity would create different degrees of ambiguity in the decision of system order and the identification of corresponding modal parameters. To conquer this difficulty, the SSI technique is typically associated with the stabilization diagram to perform the analysis for practically measured signals from civil structures. More specifically, the time lag parameter *i* is designated first and then the system order *n* displayed along the ordinate is gradually increased to identify different sets of modal frequencies plotted along the abscissa. In the stabilization diagram, the actual physical modes can be clearly distinguished from the spurious mathematical modes by the fact that they would basically group together in separated narrow neighborhoods of stable frequency values.

The authors recently explored the SSI application in stay cables where the conventional stabilization diagram faces a great challenge (Wu *et al*. 2014, 2016). An important discovery is that the lower limit for setting the time lag parameter can be decided by the ratio of the fundamental period of cable to the sampling time increment

for a valid identification with the conventional stabilization diagram. Inspired by such a criterion, that work further proposed an alternative stabilization diagram by fixing the system order n first and then varying the time lag parameter i. It was suggested to first examine the FAS of cable signals to help an appropriate choice of the system parameter n and to determine the fundamental period of cable for setting the lower limit i_{min} of time lag parameter. In addition, the upper limit of time lag parameter is decided by the need in the subsequent processes to extract reliable modal parameters. It has been validated that the alternative stabilization diagram holds the advantage in less interference from the superfluous modes.

This concept of alternative stabilization diagram is extended to the application for analyzing the vibration measurements of bridge deck in the current study. As mentioned in the previous section, the investigation of the mode identifiability problem will be concentrated on the three major modes (BV1, CT, and BH1) of Ting Kau Bridge. Consequently, the examined frequency range in the following analysis will be focused from 0 to 0.5 Hz. Moreover, the system order is fixed at $n = n_0 = 20$ considering that around 10 peaks can be clearly observed from the FAS of different deck measurements in this frequency range. As illustrated in Fig. 4, the frequency of the first and most dominant mode is about 0.165 Hz (i.e., with a period of 6.1 sec). Considering the sampling frequency at 25.6 Hz (i.e., Δt = 0.039 sec), $i \geq i_{min}$ = 6.1/0.039 = 160 is accordingly taken as the criterion for an appropriate choice of the time lag parameter in this case. Hence, the SSI analysis is then performed with the time lag parameter increasing from i_{min} = 160 to $i_{max} = i_{min} + \Delta i$ = 300 with the range of Δi = 140 to establish the alternative stabilization diagrams shown in Figs. 5(a) and 5(c) for the two selected cases N1 and Sam under different wind conditions. The corresponding Fourier amplitude spectra are also shown in the background of these figures. It can be seen that the alternative stabilization diagram of Case N1 is relatively not as clean as those of Case Sam to indicate a little stronger interference from the superfluous modes.

Even enhanced with the alternative stabilization diagram to provide a better foundation for effective modal identification, the task of extracting reliable modal parameters from this diagram requires further efforts. A robust algorithm was also developed in a recent study (Wu *et al*. 2016) to carry out three stages of hierarchical sifting process for gathering close values in all the three caterories of modal parameter including frequencies, damping ratios, and mode shape vectors. The first stage of hierarchical sifting process starts with sorting all the identified frequency values exhibited in the stabilization diagram in an ascending order. To systematically extract the clustered groups of frequency values, a simple clustering index was defined by taking the span of any adjacent L frequency values. With this operation, the extraction of all the locally clustered frequency values can be conveniently accomplished by merely searching for all the local minima. Certain criterion Δf can be further imposed to guarantee each extracted group of frequency values would reach a specified level of concentration. With L = 100 and Δf = 0.005 Hz (1% of the total frequency range examined in the stabilization diagram), a few groups of clustered frequency values as shown in Figs. 5(b) and 5(d) can be extracted from Figs. 5(a) and 5(c). It is obvious that the somewhat filthy diagrams in Figs. 5(a) and 5(c) are cleaned to produce well clustered groups symbolized by blue cross signs in Figs. 5(a) and 5(c) at the end of this stage.

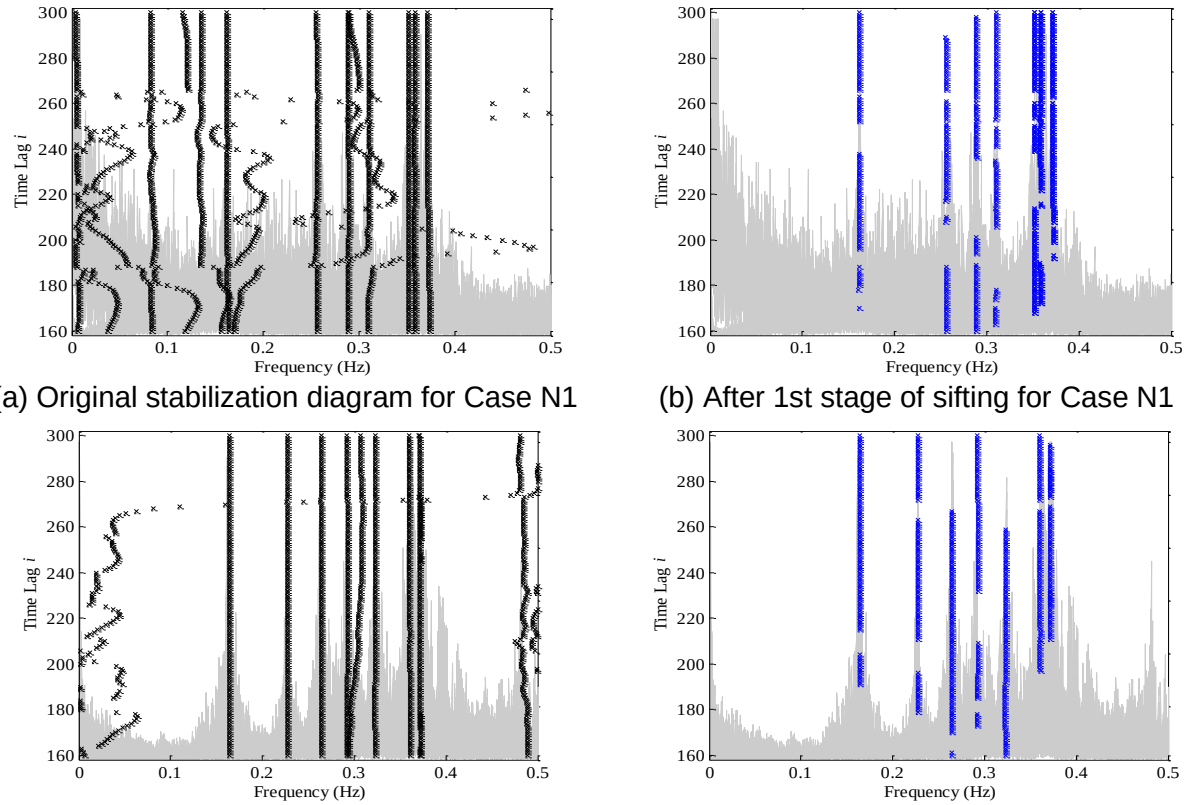

(a) Original stabilization diagram for Case N1 (b) After 1st stage of sifting for Case N1

(c) Original stabilization diagram for Case Sam (d) After 1st stage of sifting for Case Sam

Fig. 5 Alternative stabilization diagram and results after 1st sifting stage

For each group surviving from the first stage, all the damping ratios corresponding to its $L=100$ frequency values are further sifted in the second stage with the same techniques as adopted in the first stage to filter $L/2$ = 50 most closed values. The $L/2$ = 50 frequency values and their corresponding damping ratios of each mode surviving the second stage finally go to the third stage for examining the consistency of their corresponding mode shape vectors. A consistency index was defined (Wu *et al*. 2016) by taking the norm (or length) for the difference of any two mode shape vectors. It should be especially emphasized that each mode shape vector has to be normalized into unit length such that the comparison can be made on the same basis. For each group of L_1 (L_1 = $L/2$ =50 in the beginning) mode shape vectors, a $L_1 \times L_1$ symmetric consistency matrix with zero diagonal elements can be obtained. The average of all the elements in each row (or column) of this consistency matrix except for the diagonal element is then adopted to represent the average distance of each normalized mode shape vector to the other L_1-1 ones in the same group. Such an average is thus referred as the average distance and used to further carry out the third stage of sifting process on the mode shape vectors. In this work, 1% is taken as the shifting criterion. The 50 (or less) normalized shape vectors of modes BV1 and BH1 passing the three stages of sifting are plotted in Fig. 6. The shape vectors of these two modes can be consistently identified under different wind conditions. Figs. 6(a) and 6(c) confirm that

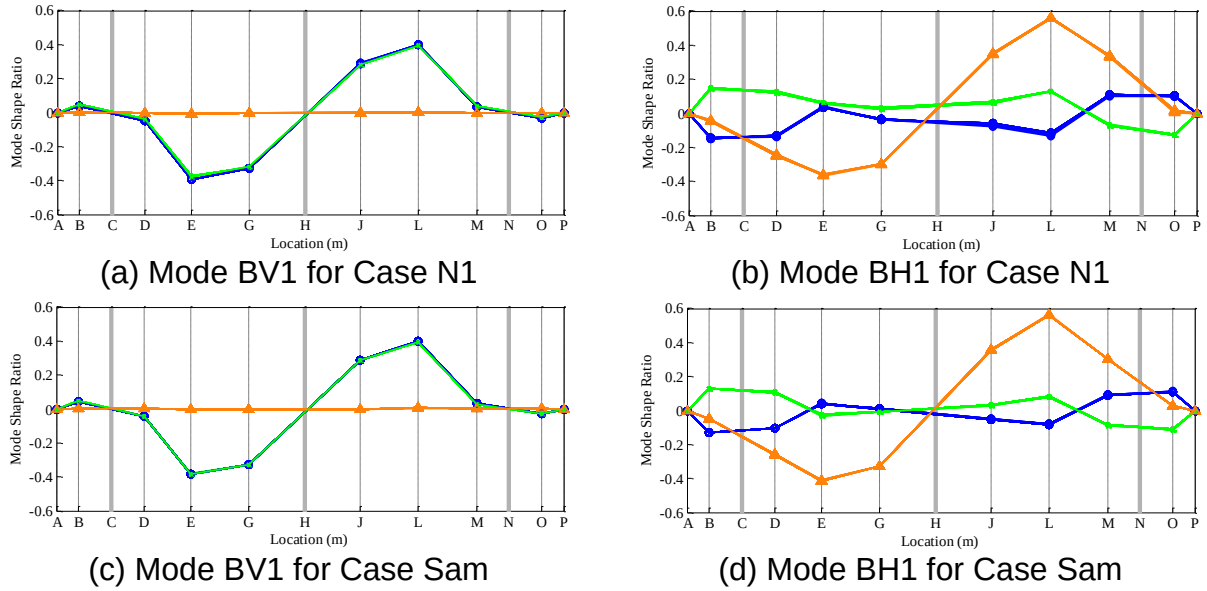

(a) Mode BV1 for Case N1

(b) Mode BH1 for Case N1

(c) Mode BV1 for Case Sam

(d) Mode BH1 for Case Sam

Fig. 6 Normalized shape vectors of modes BV1 and BH1 under various wind conditions

BV1 is certainly a vertically bending mode with its vertical shape vectors along both sides of deck coincide with each other and its horizontal shape ratios along the central line of deck almost stay at zero. On the other hand, Figs. 6(b) and 6(d) validate that BH1 is basically a horizontally bending mode with its vertical shape ratios along both sides of deck much smaller than its horizontal shape ratios along the central line of deck in a full-sine shape. The detailed discussions for the targeted mode CT to explore the mode identifiability problem will be presented in the following sections.

5. IDENTIFIED RESULTS FROM SSI ANALYSIS

With the improved SSI algorithm to go through all the three sifting stages, the corresponding modal frequencies, damping ratios, and mode shape vectors for the 50 (or less) survivors in each clustered group are then averaged to determine the final identified modal parameters for each mode in this study. The results for Cases N1 to N6 under the normal wind condition are first listed in Table 2. The frequency values of mode BV1 for these 6 cases tightly fall between 0.162 Hz and 0.165 Hz and those of mode BH1 consistently vary from 0.257 Hz to 0.261 Hz. As for the damping ratios, the values of mode BV1 are generally around 1% and those of mode BH1 mainly range from 1% to 2% with an exception close to 4%. Regarding the mode shape vectors for these cases, they are all similar to the ones displayed in Fig. 6. Most important of all, no stable parameters of mode CT can be obtained for all the cases under the normal wind condition as demonstrated in Fig. 5(a).

The identified results for the four cases under the typhoon condition are listed in Table 3. It can be observed that the frequency values of both modes BV1 and BH1 are usually a little larger than the corresponding values identified in the cases under the normal wind condition. A reasonable explanation for this phenomenon is that the much

Table 2 Identified modal parameters for normal cases

Case	Mode BV1		Mode CT		Mode BH1	
	Frequency (Hz)	Damping Ratio (%)	Frequency (Hz)	Damping Ratio (%)	Frequency (Hz)	Damping Ratio (%)
N1	0.162	0.848	-	-	0.257	1.797
N2	0.162	1.116	-	-	0.257	1.956
N3	0.163	1.178	-	-	0.259	1.431
N4	0.164	0.853	-	-	0.258	1.227
N5	0.164	1.336	-	-	0.255	3.888
N6	0.165	1.198	-	-	0.261	0.852

Table 3 Identified modal parameters for typhoon cases

Case	Mode BV1		Mode CT		Mode BH1	
	Frequency (Hz)	Damping Ratio (%)	Frequency (Hz)	Damping Ratio (%)	Frequency (Hz)	Damping Ratio (%)
Maggie	0.167	1.544	0.227	0.676	0.263	0.913
Sam	0.164	1.844	0.227	0.317	0.264	0.789
York 1	0.165	3.036	0.227	0.513	0.260	3.894
York 2	0.166	1.671	0.226	0.617	0.260	1.431

less passing traffic under the strong wind condition would reduce the effective mass of the system to increase the modal frequencies. It is noteworthy that the identified frequencies for the other modes presented in Ni *et al*. (2015) hold the same trend. Furthermore, the most notable fact is that stable parameters of mode CT can be consistently identified for all the cases under the strong wind condition. The frequency values of this mode closely fall between 0.226 Hz and 0.227 Hz and its damping values are at the order of 0.5%. Combined with the observation under the normal wind condition, mode CT is no doubt a deficient mode that cannot be identified all the time. The 50 (or less) normalized shape vectors of mode CT passing the three stages of sifting for each typhoon case are shown in Fig. 7. For this deficient mode, its vertical shape ratios along both sides of deck distinctly move in the opposite directions to indicate a torsional vibration. Its horizontal shape ratios along the central line of deck, on the other hand, follow a half-sine shape to imply a horizontally bending mode. These two clues disclose that mode CT is a coupled mode in both the torsional and transverse directions, as specified by Ni *et al*. (2015). Further considering the concentration in the central part for major vibration of this mode in both directions and their connected

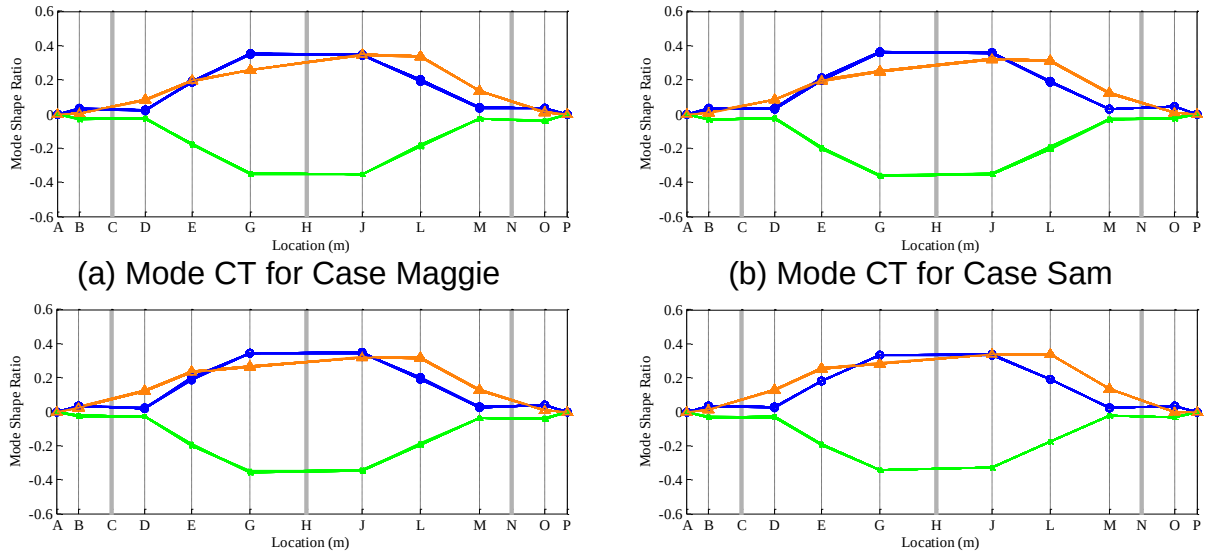

(a) Mode CT for Case Maggie

(b) Mode CT for Case Sam

(c) Mode CT for Case York 1

(d) Mode CT for Case York 2

Fig. 7 Normalized shape vectors of mode CT for different typhoon cases

geometry, a more aggressive attempt in this study is to postulate that mode CT is primarily induced by the motion of the central tower. With such a postulation, it would be straightforward to explain the strong influence of the wind condition on the identifiability of this mode. To verify this postulation, the SSI analysis will be conducted in Section 6 with the incorporation of vibration measurements at the central tower.

6. ANALYSIS FURTHER INCLUDING MEASUREMENTS AT CENTRAL TOWER

Based on close examination on the geometry of its mode shape vector, it is postulated in Section 5 that the deficient mode CT is principally induced by the motion of the central tower. To certify this postulation, the analysis with further incorporation of the acceleration records measured at the central tower is performed in this section. As illustrated in Fig. 1, two bi-axial accelerometers labeled as T1 and T2 in this work are installed at the top and the base of the central tower, respectively. The measurements of Sensors T1 and T2 in the transverse (*y*) direction are taken to conduct the analysis together with the records from the 24 uni-axial accelerometers deployed on the bridge deck.

Solid evidences can be collected from performing the SSI analysis with both the deck and tower measurements to prove that mode CT is more a tower mode than a deck mode. The identified modal parameters for the 6 cases under the weak wind condition are listed in Table 6. In contrast to Table 2 obtained from performing the SSI analysis simply with the deck measurements, stable parameters of mode CT can be identified for all the cases under the weak wind condition. In other words, mode CT can no longer be considered as a deficient mode with the addition of two tower measurements. The 50 (or less) extended shape vectors of mode CT to include the shape ratios at two tower locations for Cases N1 to N6 and the four typhoon cases are

Table 6 Identified modal parameters for normal cases including pylon measurement

Case	Mode BV1		Mode CT		Mode BH1	
	Frequency (Hz)	Damping Ratio (%)	Frequency (Hz)	Damping Ratio (%)	Frequency (Hz)	Damping Ratio (%)
N1	0.162	0.885	0.227	0.472	0.257	1.612
N2	0.162	1.018	0.226	0.761	0.258	1.724
N3	0.163	0.164	0.226	0.678	0.259	1.285
N4	0.164	0.985	0.224	1.594	0.258	1.043
N5	0.164	1.489	0.225	1.125	0.257	4.527
N6	0.165	1.163	0.226	1.850	0.261	0.806

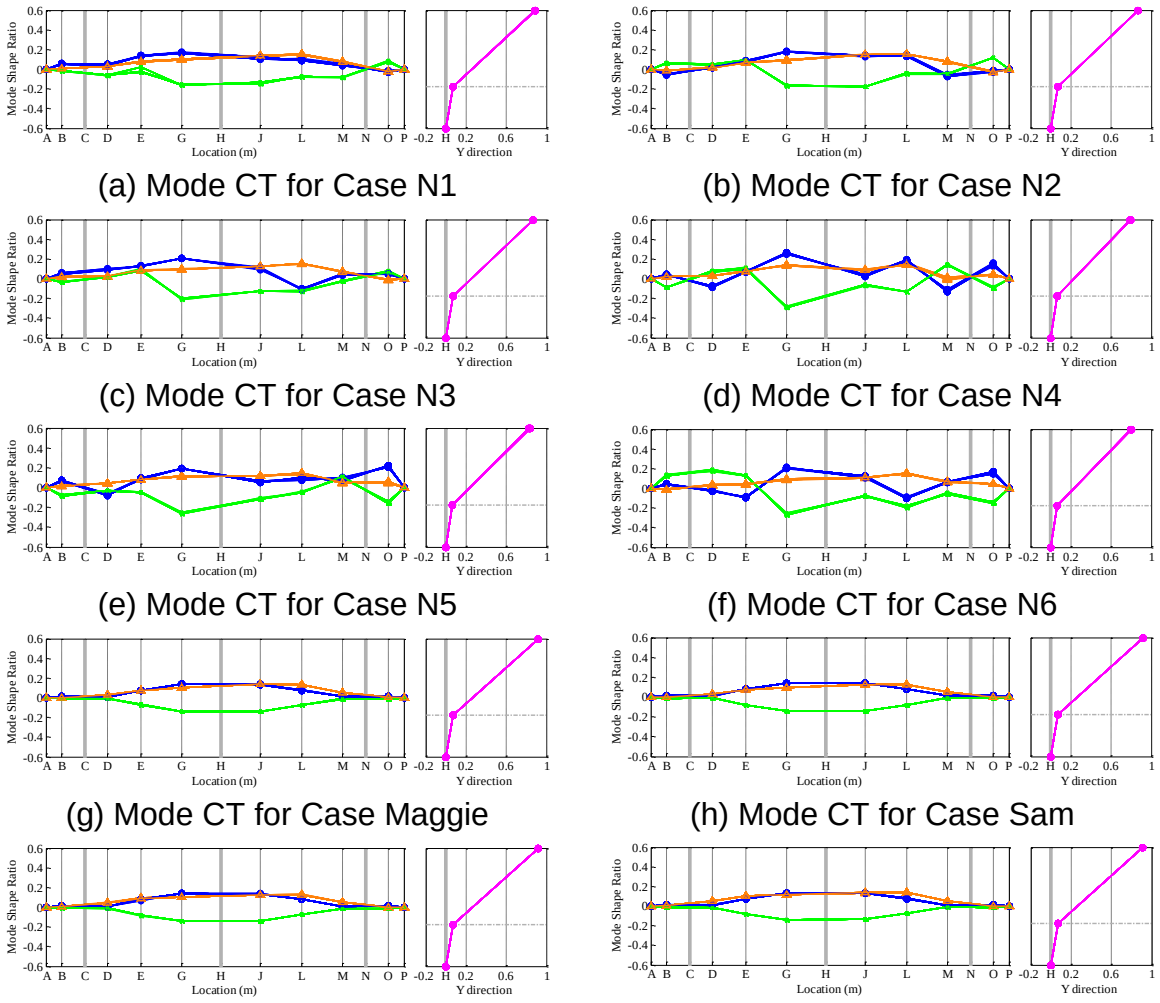

(a) Mode CT for Case N1

(b) Mode CT for Case N2

(c) Mode CT for Case N3

(d) Mode CT for Case N4

(e) Mode CT for Case N5

(f) Mode CT for Case N6

(g) Mode CT for Case Maggie

(h) Mode CT for Case Sam

(i) Mode CT for Case York 1

(j) Mode CT for Case York 2

Fig. 8 Extended mode shape vectors of mode CT for different wind conditions

also drawn in Fig. 8. The in-scale plots in Fig. 8 evidently demonstrate that the dominance of tower motion at the top for mode CT. More specifically, the largest shape ratio at deck for this mode is merely around 14% of that at the tower top in the four typhoon cases with consistent mode shape vectors. As for the 6 cases under the weak wind conditions, the mode shape ratios at deck locations may mildly change in different cases compared to the corresponding steady values at tower locations. More precisely, the transverse mode shape ratios along the central line of deck are relatively more stable than the vertical mode shape ratios at both sides of deck in these cases. All the above observations point to the direction that an effective consideration of mode CT should cover both the tower and deck components of this bridge. To clearly express the vibration mechanism of this mode, it can be conveniently pictured as the transversely bending motion of the central tower to simultaneously induce the transversely bending and torsional motions of the connected deck.

7. CONCLUSIONS

Focused on a deficient mode that cannot be always identified from the monitoring data of Ting Kau Bridge under different wind conditions, this study explores the mode identifiability problem in conducting the operational modal analysis with ambient vibration measurements. The evaluation of delicately selected cases clearly distinguishes the effect of traffic excitation on the identifiability of the targeted deficient mode from the effect of wind excitation. Further efforts are dedicated in the present work to carefully inspect the shape vector of the deficient mode under different excitation conditions. Such an examination leads to the postulation that this mode is actually induced by the motion of the central tower. This postulation explains the strong dependence of identifiability on the wind excitation for the deficient mode, which is not supposed to occur in the modes majorly with deck vibration. The SSI analysis incorporating the tower measurements solidly verifies this postulation by yielding the prevailing components at the tower locations in the extended mode shape vector. Moreover, it is also confirmed that this mode can be stably identified under all the circumstances with the addition of tower measurements to remove the tag of deficient mode. An important lesson learned from this discovery is that the problem of mode identifiability usually comes from the lack of appropriate measurements taken at the right locations.

REFERENCES

Ni, Y.Q., Wang, Y.W. and Xia, Y.X. (2015), “Investigation of mode identifiability of a cable-stayed bridge: comparison from ambient vibration responses and from typhoon-induced dynamic responses”, *Smart Struct. Syst.*, **15**(2), 447-468.

Peeters, B. (2000), “System identification and damage detection in civil engineering”, Ph.D. Dissertation, Katholieke Universiteit Leuven, Leuven.

Reynders, E., Houbrects, J. and De Roeck, G. (2012), “Fully automated (operational) modal analysis”, *Mech. Syst. Signal Pr.*, **29**, 228-250.

Ubertini, F., Gentile, C. and Materazzi, A.L. (2013), “Automated modal identification in operational conditions and its application to bridges”, *Eng. Struct.*, **46**, 264-278.
Van Overschee, P. and De Moor, B. (1991), “Subspace algorithm for the stochastic identification problem”, *Proceedings of the 30th IEEE Conference on Decision and Control*, Brighton, England.
Wu, W.H., Chen, C.C., Wang, S.W. and Lai, G. (2014), “Modal parameter determination of stay cable with an improved algorithm based on stochastic subspace identification”, *Proceedings of 7th European Workshop on Structural Health Monitoring*, Nantes, France.
Wu, W.H., Wang. S.W., Chen, C.C. and Lai, G. (2016), “Application of stochastic subspace identification for stay cables with an alternative stabilization diagram and hierarchical sifting process”, *Struct. Control Health Monit.*, DOI: 10.1002/stc.1836.